Resonant Harmonic Generation and Dynamic Screening in a Double Quantum Well

J. N. Heyman, K. Craig, B. Galdrikian, M. S. Sherwin, K. Campman, P. F. Hopkins, S. Fafard,
and A. C. Gossard

Quantum Institute, University of California at Santa Barbara, Santa Barbara, California 93106
and Materials Department, University of California at Santa Barbara, Santa Barbara, California 93106

Second- and third-harmonic generation are observed in a semiconductor heterostructure which approximates a two-state system with an 11-meV level spacing. A resonance in the second- (third-) harmonic generation is found when the depolarization-shifted infrared absorption peak is Stark tuned through 2 (3) times the pump frequency. These resonances are thus associated with the depolarization-shifted, and not the bare, intersubband energy. Data are analyzed with a theory of second-harmonic generation including dynamic screening. Saturation is observed at pump intensities > 10 kW/cm^2.

Harmonic generation and other optical nonlinearities in dilute quantum systems are well understood in terms of a diagrammatic form of time-dependent perturbation theory [1–3]. However, in systems of charged particles in which many-body effects are important, the susceptibilities must be obtained self-consistently. The effect of this dynamic screening on the linear response is well known. In ionic crystals it leads to the shift of the infrared absorption due to lattice modes from the transverse to the longitudinal optic phonon frequency. In quantum wells, dynamical screening leads to a depolarization shift between the intersubband spacing and the intersubband infrared absorption resonance [4,5]. The effect of dynamic screening on the nonlinear optical properties of materials has not been thoroughly investigated.

Quantum wells in semiconductors are model systems for the study of the interactions of light with matter. West and Eglash [6] have observed large oscillator strengths associated with intersubband transitions. More recently, Gurnick [7] and Yuh [8] predicted that asymmetric quantum well would display giant second-order electric susceptibilities. This has been supported by measurements of resonant second-harmonic generation [9,10] and optical rectification [10] in AlGaAs/GaAs asymmetric wells. In addition, large third-order susceptibilities in asymmetric wells have been observed through measurements of the intensity-dependent refractive index [11], and third-harmonic generation [12]. The systems studied did not show measurable depolarization shifts because the Coulomb and exchange self-energies of electrons in the wells (< 10 meV) were much smaller than the subband spacings ($E_{12} \approx 124$ meV). Bewley *et al.* [13] have shown that nonresonant second-harmonic generation can be observed from quantum wells having intersubband resonances in the far-infrared (FIR), in which the electron-electron interaction cannot be neglected. In this Letter, we present our study of resonant harmonic generation in a semiconductor heterostructure which displays a substantial depolarization shift. We compare the frequency, strength, and line shape of the resonance in

second-harmonic generation to a self-consistent theory of second-harmonic generation including dynamic screening effects, and find an excellent agreement between theory and experiment.

The structure studied consists of a single period of a modulation-doped asymmetric double quantum well, with 85 and 75 Å GaAs wells separated by a 25 Å Al$_{0.3}$Ga$_{0.7}$As barrier. It was grown by molecular beam epitaxy on a semi-insulating GaAs substrate. The barrier region on either side of the wells consists of 5200 Å of a Al$_{0.3}$Ga$_{0.7}$As digital alloy consisting of a 20 Å period superlattice (14 Å GaAs and 6 Å AlAs). The low temperature ($T < 50$ K) charge density and electron in-plane mobility in the well measured by Hall effect are 2×10^{11} cm^{-2} and 1.0×10^5 cm^2/Vs. Photoluminescence (PL) and photoluminescence excitation measurements performed near 4.2 K were used to determine the intersubband spacings. In our asymmetric structure both the E_1-HH$_1$ (heavy-hole) and E_2-HH$_1$ PL transitions are allowed. An electron subband spacing $\hbar\omega_{12} = 11$ meV was extracted directly from the spacing between these transitions, without reference to the hole subband energies.

For further measurements, a Schottky gate was evaporated on the surface of the structure, and Ohmic contacts were made to the double well. A negative voltage between the gate and Ohmic contacts imposes a dc electric field across the structure and depletes it of charge. Measurements of capacitance versus gate voltage $[C(V_g)]$ determine that the well is fully depleted at -1.6 V bias ($E = 15$ kV/cm). Aluminum was also evaporated on the substrate side of the wafer, so that the sample formed a parallel-plate waveguide. In our linear and nonlinear optical experiments, polarized FIR radiation was coupled into the edge of the wafer with E parallel to the growth direction.

The linear absorption was measured in the sample at 1.4 K using a Bomem DA3.002 Fourier transform spectrometer equipped with a 1.4 K Ge bolometer. Transmission spectra were measured as a function of gate bias, and the absorbance was computed using the transmit-
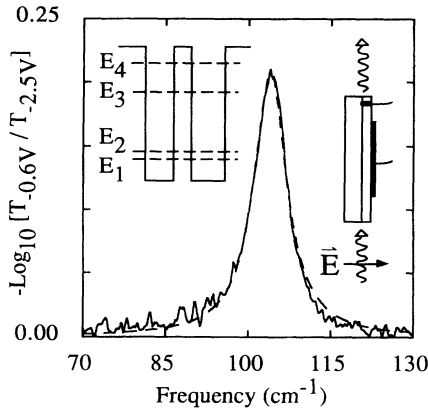
FIG. 1. Far-infrared absorption spectrum of the asymmetric double well at $T = 1.4$ K. Dashed line is a fit by a Lorentzian. Inset: Conduction band diagram showing the subband energies. The absorption peak corresponds to excitation between the two lowest subbands. Drawing shows optical coupling geometry.
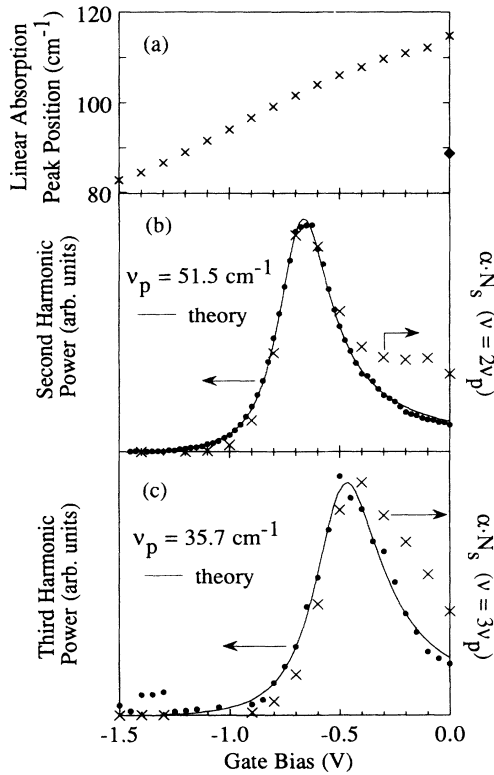

FIG. 2. (a) (×) Absorption peak position $v_{12}^* = \omega_{12}^*/2\pi c$ versus gate bias. (♦) Bare intersubband frequency v_{12} determined from photoluminescence measurements at 0 V bias. (b) Second-harmonic power versus gate bias (●) at $T < 15$ K. Theory is a fit to our calculated line shape [Eq. (4)]. Crosses show absorption coefficient α times charge density N_s measured at 2 times pump frequency v_p. (c) Third-harmonic power versus gate bias (●) at $T < 15$ K. Theory is a fit by product of a Lorentzian and the square of the charge density. (×) The product $\alpha(3v_p)N_s$ is also shown.

tance of the fully depleted sample as a reference. The absorption spectrum between 5 and 200 cm^{-1} consists of a single line with an approximately Lorentzian line shape, as shown in Fig. 1. At 0 V gate bias the peak position is $\hbar\omega_{12}^* = 14.3$ meV (115 cm^{-1}), and the full width at half maximum is 0.55 meV. Figure 2(a) shows an approximately linear Stark shift of the peak of 0.29 meV cm/kV [(2.7 meV)/V_{applied}].

Nonlinear optics experiments employed the UCSB free-electron laser (FEL) [14] as a quasi-cw FIR pump. The sample was mounted in a variable-temperature cryostat and measurements were performed at $T < 15$ K. A waveguide cutoff type [15] high-pass filter was used to separate the weak harmonic radiation from the strong transmitted fundamental. The frequency and intensity of the harmonic radiation were measured with a scanning Fabry-Pérot spectrometer and a 4.2 K Ge bolometer. The experiment was performed in a N$_2$ atmosphere to reduce absorption due to water vapor.

Figure 2(b) shows resonant second-harmonic generation (SHG), observed by illuminating the sample with the FIR laser at a fixed frequency and using gate bias to tune the intersubband spacing [16]. A well-defined resonance is observed at $V_g = -0.67$ V when the pump frequency is 51.5 cm^{-1}. At this bias the laser frequency is $\frac{1}{2}$ the frequency of the linear absorption peak ($\hbar\omega_{12}^* = 2\hbar v_{\text{pump}}$). Figure 3 shows the second-harmonic intensity at resonance at pump intensities inside the sample up to 100 kW/cm^2. Below 10 kW/cm^2, the SH power is proportional to the second power of the pump intensity. Saturation of the SH power is observed at higher intensities. We also observe changes in the resonance line shape and peak position at high intensity, and these results will be discussed elsewhere.
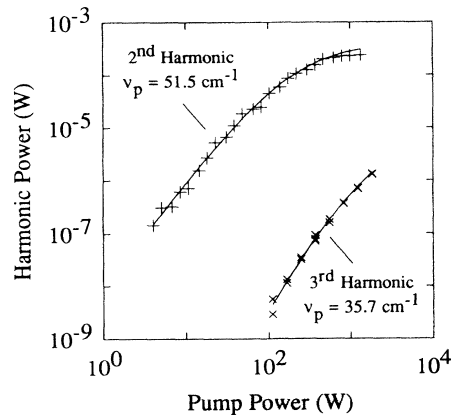

FIG. 3. Second-harmonic and third-harmonic powers versus pump power at resonance ($V_g = -0.67$ V). The powers are not corrected for losses in the cryostat optics. Solid line is a fit by a model involving saturation of nonresonant intersubband absorption (see text). The maximum pump intensity at the sample was 110 ± 40 kW/cm^2 and 70 ± 40 kW/cm^2 for second- and third-harmonic generation, respectively.

Figure 2(c) shows resonant third-harmonic generation in our asymmetric double quantum well under FEL illumination at 35 cm^{-1}. The third-harmonic resonance occurs when the system is tuned so that the laser frequency is $\frac{1}{3}$ the frequency of the infrared absorption peak ($\hbar\omega_{12}^* = 3h\nu_{pump}$). The dependence of the third-harmonic power on the pump power is subcubic at high pump powers, as shown in Fig. 3.

We have calculated the energies and envelope functions of electrons at the subband minima in our double well by self-consistently solving the Schrödinger and Poisson equations, taking into account the exchange-correlation energy within the local density approximation. Assuming free motion in the plane of the well, we may separate out the dynamics in the well's growth direction, giving the one-dimensional Schrödinger equation

$$\left[-\frac{\hbar^2}{2m^*}\frac{d^2}{dz^2} + V_{\text{eff}}(z) \right]\xi_n(z) = E_n\xi_n(z) , \tag{1}$$

where m^* is the effective mass, E_n is the energy at the bottom of the nth subband, and

$$V_{\text{eff}}(z) = v_0(z) + v_s[n(z);z] + v_{xc}[n(z);z] \tag{2}$$

is the effective single-particle potential. The conduction band without electron-electron interactions is given by $v_0(z)$, while $v_s[n(z);z]$ is due to the direct Coulomb repulsion between electrons, and $v_{xc}[n(z);z]$ is the exchange-correlation term. Equations (1) and (2) may be solved self-consistently to give the envelope functions of the electrons at the subband minima.

The calculated subband spacings at 0 V bias are $E_{12} = 11.9$ meV, $E_{13} = 110$ meV, and $E_{14} = 156$ meV, where

$E_{nm} = E_n - E_m$. Since $E_{12} \ll E_{13}$, the polarizability of a single electron in the quantum well potential under excitation at energies $h\nu$ of the order or less than E_{12} can be calculated using time-dependent perturbation theory for a two-state system. Contributions from higher subbands will be too small to measure. However, calculation of the macroscopic susceptibility at finite charge density is more complex. One must self-consistently account for the change in the effective single-particle potential (which includes Coulomb and exchange-correlation effects) arising from the time-dependent charge density. This calculation has been performed for the first-order ac conductivity [4,5]. To calculate the second-harmonic susceptibility, we have carried this self-consistent treatment out to second order [17].

We assume that in the system's initial state, only the ground subband is occupied. When an external perturbation $eE_{\text{ext}}(z)\cos(\omega t)$ is applied, it modifies the charge density as $\Delta n^{(1)}(z)\cos(\omega t) + \Delta n^{(2)}(z)\cos(2\omega t)$. We do not need to include the static modification to the charge density since it does not affect the first or second harmonic, to within second order. Self-consistency is obtained by demanding that this change in density both arise from and also generate the second-order perturbing potential

$$V(z,t) = \sum_{j=1}^{2} [eE_{\text{FIR}}z\delta_{j,1} + \Delta v_s^{(j)}(z) + \Delta v_{xc}^{(j)}(z)]\cos(j\omega t) . \tag{3}$$

The potentials $\Delta v_s^{(j)}(z)$ and $\Delta v_{xc}^{(j)}(z)$ are the changes in the direct or Coulomb potential and the exchange-correlation potential, respectively, and are treated as functionals of $\Delta n^{(j)}(z)$. For a two-state system, the result of this calculation is

$$\chi_s^{(2)}(2\omega;\omega,\omega) = 3N_s z_{21}^2 z_{22}\frac{e^3}{\hbar^{-2}}\frac{(\omega_{12}+i\Gamma)^2[(\omega_{12}+i\Gamma)^2 - \omega^2]}{[(\omega_{12}^*+i\Gamma)^2 - 4\omega^2][(\omega_{12}^*+i\Gamma)^2 - \omega^2]^2} , \tag{4}$$

where the dipole matrix element $z_{nm} = \langle \xi_n | z | \xi_m \rangle$ is calculated with the origin such that $z_{11} = 0$, and we have inserted the phenomenological dephasing time $1/\Gamma$. We use the convention $P^{(2)} = \chi^{(2)}E^2$. The second-order susceptibility has a second-order pole at the depolarization-shifted frequency $\omega = \pm\omega_{12}^*$ and a first-order pole at $2\omega = \pm\omega_{12}^*$. Our calculation shows that this frequency is exactly equal to the resonance frequency for the first-harmonic response in the two-state approximation [5]. The well known single-particle result is a special case of Eq. (4) obtained in the limit $\omega_{12} = \omega_{12}^*$, and has simple poles at the bare frequencies $\omega = \pm\omega_{12}$ and $2\omega = \pm\omega_{12}$. We have calculated $\chi_s^{(2)}(2\omega;\omega,\omega)$ from Eq. (4) using experimentally determined values of N_s, ω_{12}^*, Γ, z_{21}, and ω_{12} at $V_g = -0.67$ V. $N_s = 1.2\times10^{11}$ cm^{-2} was determined by $C(V_g)$. The values $\hbar\omega_{12}^* = 12.77$ meV and $\Gamma = 0.42$ meV were taken from the frequency and linewidth of the infrared absorption peak, and $z_{21} = 64$ Å was obtained from the absorption coefficient at resonance us-

ing $\alpha = 4\pi\omega N_s e^2 z_{12}^2/c\sqrt{\varepsilon}a\hbar\Gamma$, where a is the thickness of the sample. Interpolating between measured values of ω_{12} at $V_g = 0$ V (from PL) and at $V_g = -1.6$ V, where the charge density is vanishing and $\omega_{12} = \omega_{12}^*$, we find a bare intersubband spacing at $V_g = -0.67$ V of $\hbar\omega_{12} = 10.65$ meV. The matrix element $z_{22} = 16.4$ Å is taken from our simulation.

The calculation may be compared to the measured sheet second-order susceptibility at resonance $\chi_s^{(2)}(2\omega; \omega,\omega)$. Assuming uniform illumination across the edge of our structure, the pump radiation couples only to the transmission electron micrograph waveguide mode of the sample. The nonlinear polarization of the charge in the well couples equally to all waveguide modes of index $m \ll a/w$, where a is the thickness of the substrate and w is the width of the quantum well. The intensity at the end of the sample at $n\omega$ due to the nth-order-harmonic generation is then given by

$$I_{n\omega} = (n\omega l)^2 \left[\frac{2\pi}{c\sqrt{\varepsilon_\omega}}\right]^{n+1} \frac{\sqrt{\varepsilon_\omega}|\chi_s^{(n)}(n\omega)|^2}{\sqrt{\varepsilon_{n\omega}}a^2} I_\omega^n \left[\frac{\sin^2(\Delta k_0 l/2)}{(\Delta k_0 l/2)^2} + 2\sum_{m=1}^{\infty} \frac{k_{n\omega}^{(0)}\sin^2(\Delta k_m l/2)}{k_{n\omega}^{(m)}(\Delta k_m l/2)^2}\right], \tag{5}$$

where l is the length of the sample, I_ω is the intensity of the pump beam inside the sample, $k_{n\omega}^{(m)}$ is the propagation constant of radiation at $n\omega$ traveling in waveguide mode m, and $\Delta k_m = k_{n\omega}^{(m)} - nk_\omega$. We find for both second- and third-harmonic generation that there exists a mode for which $\Delta k_m \approx 0$, so that harmonic generation in this mode is phase matched. This type of phase matching was first exploited to achieve phase-matched harmonic generation in bulk GaAs by Anderson and Boyd [18]. The principal source of error in our susceptibility measurements is the uncertainty in the absolute pump and second-harmonic powers at the sample. Summarizing the measured and calculated results, the measured $\chi_s^{(2)}(\omega_{12}^*;\omega_{12}^*/2,\omega_{12}^*/2) = (4\pm2)\times10^{-8}$ cm^2/statvolt, while the calculated value is 5.4×10^{-8} cm^2/statvolt. The third-order susceptibility at resonance is $\chi_s^{(3)}(\omega_{12}^*;\omega_{12}^*/3,\omega_{12}^*/3,\omega_{12}^*/3) = (3\pm1.5)\times10^{-9}$ cm^3/statvolt^2. The calculated and measured magnitudes of $\chi_s^{(2)}(2\omega,\omega,\omega)$ at $2\omega = \omega_{12}^*$ agree within error, and the experimental data give an excellent fit with the calculated line shape (Fig. 2). The linear absorption and second-harmonic data can also be compared directly. Near resonance at $2\omega = \omega_{12}^*$, the second-harmonic power at a pump frequency v_p should be proportional to the absorption coefficient at $2v_p$ times the charge density, $P_{2\omega}(V_g,v_p) \propto \alpha(V_g,2v_p)N_s$. Experimentally, it is found that the resonance positions agree to within ±0.05 V (±0.1 meV), where the uncertainty arises from a small run-to-run irreproducibility in the charge density, and possible shifts in the resonance energy due to the temperature difference between the two measurements.

Our data show saturation of the harmonic generation at pump powers > 10 kw/cm^2. Assuming any absorption by the carriers, saturation is expected at sufficiently high pump powers as the electron population becomes equally distributed between the two subbands. We calculate that nonresonant single-photon absorption from the tail of the intersubband absorption will be the dominant absorption mechanism at the pump intensities we have investigated. In Fig. 3 we fit the intensity dependence of the second- and third-harmonic power by a standard expression for the saturation of the susceptibilities in a two-level system [3] using an intersubband relaxation time of order 20 ps.

In conclusion, we have designed and studied an asymmetric double-quantum-well structure which exhibits extremely large nonlinear susceptibilities in the far infrared. The physical system is well controlled, approximating a two-level system. This has allowed us to study resonant second- and third-harmonic generation in a single heterostructure in which many-electron effects are important. We find that resonances in the nonlinear susceptibilities for harmonic generation occur when the frequency of the generated light equals the frequency of the depolarization-shifted resonance ($\hbar\omega_{12}^*$), and not the bare intersub-

band spacing. The second-harmonic generation is in good agreement with a model which self-consistently includes dynamic screening of the ac fields by polarization of the charge. Our results suggest that resonances in nonlinear susceptibilities may always be associated with the depolarization shifted resonances in linear absorption. However, more work is required to verify this. In addition, saturation of the harmonic power occurs at high pump intensities, probably due to nonresonant intersubband absorption.

[1] J. F. Ward, Rev. Mod. Phys. **37**, 1 (1965).

[2] T. K. Yee and T. K. Gustafson, Phys. Rev. A **18**, 1597 (1978).

[3] Y. R. Shen, *The Principles of Nonlinear Optics* (Wiley, New York, 1984).

[4] S. J. Allen, D. C. Tsui, and B. Vinter, Solid State Commun. **20**, 425 (1976).

[5] T. Ando, A. B. Fowler, and F. Stern, Rev. Mod. Phys. **54**, 436 (1982).

[6] L. C. West and S. J. Eglash, Appl. Phys. Lett. **46**, 1156 (1985).

[7] M. K. Gurnick and T. A. DeTemple, IEEE J. Quantum Electron. **19**, 791 (1983).

[8] P. F. Yuh and K. L. Wang, J. Appl. Phys. **65**, 4377 (1989).

[9] M. M. Fejer, S. J. B. Yoo, R. L. Byer, A. Harwit, and J. S. Harris, Jr., Phys. Rev. Lett. **62**, 1041 (1989).

[10] E. Rosencher and P. Bois, Phys. Rev. B **44**, 11315 (1991).

[11] A. Sa'ar, N. Kuze, J. Feng, I. Grave, and A. Yariv, in *Intersubband Transitions in Quantum Wells*, edited by E. Rosencher, B. Vinter, and B. Levine (Plenum, New York and London, 1992), p. 197.

[12] C. Sirtori, F. Capasso, D. L. Sivco, and A. Y. Cho, Phys. Rev. Lett. **68**, 1010 (1992).

[13] W. W. Bewley *et al.*, Phys. Rev. B **48**, 2376 (1993).

[14] G. Ramian, Nucl. Instrum. Methods Phys. Res., Sect. A **318**, 225 (1992).

[15] F. Keilmann, Infrared Phys. **31**, 373 (1991).

[16] C. Sirtori, F. Capasso, D. L. Sivco, A. L. Hutchinson, and A. Y. Cho, Appl. Phys. Lett. **60**, 151 (1992).

[17] B. Galdrikian (unpublished).

[18] D. B. Anderson and J. T. Boyd, Appl. Phys. Lett. **19**, 266 (1971).